Report

Cell Reports

KCC2-Mediated Cl^- Extrusion Modulates Spontaneous Hippocampal Network Events in Perinatal Rats and Mice

Graphical Abstract

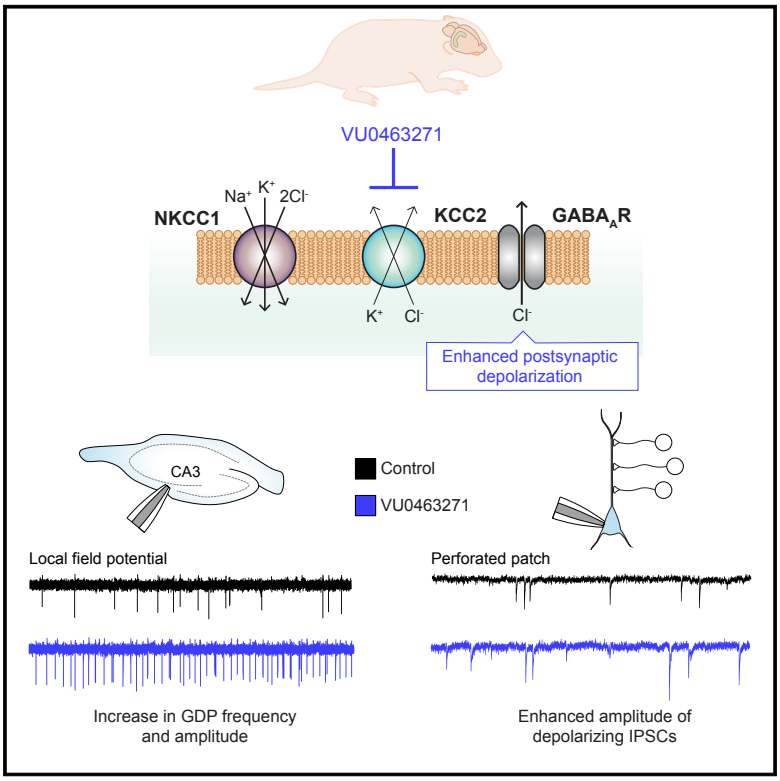

Highlights

- Transport-functional KCC2 is present in perinatal CA3 pyramidal neurons
- KCC2 restrains depolarizing synaptic GABAergic drive onto CA3 pyramidal neurons
- KCC2-mediated Cl^- extrusion regulates pyramidal neuron spiking and synchronization
- KCC2 regulates GDPs already at their developmental onset

Authors

Inkeri Spoljaric, Albert Spoljaric, Martina Mavrovic, Patricia Seja, Martin Puskarjov, Kai Kaila

Correspondence

kai.kaila@helsinki.fi

In Brief

Immature hippocampal pyramidal neurons are thought to lack chloride extrusion mediated by K-Cl cotransporter KCC2. Spoljaric et al. demonstrate that KCC2 restrains the depolarizing GABAergic synaptic drive onto CA3 pyramidal neurons in perinatal mice and rats and thereby regulates spontaneous hippocampal network events (GDPs) from their developmental onset.

Spoljaric et al., 2019, Cell Reports *26*, 1073–1081
January 29, 2019
https://doi.org/10.1016/j.celrep.2019.01.011

CellPress

Cell Reports
Report

KCC2-Mediated Cl^- Extrusion Modulates Spontaneous Hippocampal Network Events in Perinatal Rats and Mice

Inkeri Spoljaric,[1] Albert Spoljaric,[1,2] Martina Mavrovic,[1,2] Patricia Seja,[1] Martin Puskarjov,[1] and Kai Kaila[1,3,*]
[1]Faculty of Biological and Environmental Sciences, Molecular and Integrative Biosciences and Neuroscience Center (HiLIFE), University of Helsinki, 00014 Helsinki, Finland
[2]These authors contributed equally
[3]Lead Contact
*Correspondence: kai.kaila@helsinki.fi
https://doi.org/10.1016/j.celrep.2019.01.011

SUMMARY

It is generally thought that hippocampal neurons of perinatal rats and mice lack transport-functional K-Cl cotransporter KCC2, and that Cl^- regulation is dominated by Cl^- uptake via the Na-K-2Cl cotransporter NKCC1. Here, we demonstrate a robust enhancement of spontaneous hippocampal network events (giant depolarizing potentials [GDPs]) by the KCC2 inhibitor VU0463271 in neonatal rats and late-gestation, wild-type mouse embryos, but not in their KCC2-null littermates. VU0463271 increased the depolarizing GABAergic synaptic drive onto neonatal CA3 pyramidal neurons, increasing their spiking probability and synchrony during the rising phase of a GDP. Our data indicate that Cl^- extrusion by KCC2 is involved in modulation of GDPs already at their developmental onset during the perinatal period in mice and rats.

INTRODUCTION

Giant depolarizing potentials (GDPs) are the most pronounced network activity pattern in the perinatal mouse and rat hippocampus (Ben-Ari et al., 1989, 2007; Sipilä et al., 2005; Spoljaric et al., 2017; Griguoli and Cherubini, 2017). With CA3 as their pacemaker region (Sipilä et al., 2005), GDPs target neighboring areas and propagate along the septo-temporal axis of the developing hippocampus (Leinekugel et al., 1998; Ben-Ari et al., 2007). These remarkable spatiotemporal properties point to a crucial role for GDPs in the activity-dependent establishment of the evolutionarily encoded framework of hippocampal connectivity, akin to spontaneous activity in, for instance, the developing visual system (cf. Blankenship and Feller, 2010). GDPs are driven by the intrinsic pacemaker properties of CA3 pyramidal neurons and by the synergistic actions of glutamate and depolarizing GABA (Ben-Ari et al., 1989, 2007; Sipilä et al., 2005; Khazipov et al., 2015; Griguoli and Cherubini, 2017; Kirmse et al., 2018). The depolarizing GABAergic drive onto pyramidal neurons (Ben-Ari et al., 1989, 2007) is brought about by active uptake of Cl^- by the Na-K-2Cl cotransporter NKCC1 (Dzhala et al., 2005; Sipilä et al., 2006, 2009; Spoljaric et al., 2017). In the rat hippocampus, GDPs disappear by the end of the second postnatal week (Khazipov et al., 2004; Tyzio et al., 2007; Ben-Ari et al., 2007), in parallel with the increasing expression of hippocampal KCC2, the consequent fall in intraneuronal Cl^- concentration, and the negative shift in E_{GABA} (Rivera et al., 1999; Tyzio et al., 2007; Kaila et al., 2014). However, $GABA_AR$ signaling has been shown to exert dual, enhancing and suppressing, effects on hippocampal network events as early as postnatal day (P) 0–P2 in the rat (Khalilov et al., 1999; Lamsa et al., 2000). Notably, pharmacological blockade of $GABA_ARs$ results in the emergence of interictal-like network activity in the neonatal rat and fetal macaque (Khalilov et al., 1997b, 1999; Lamsa et al., 2000; Khazipov et al., 2001). This indicates that, in addition to providing a depolarizing drive, GABAergic inputs onto hippocampal pyramidal neurons mediate shunting inhibition of glutamatergic currents during GDPs (Khalilov et al., 2015). However, as explained in detail elsewhere (Kaila et al., 2014), effective shunting is sustainable in a neuron only if there is a mechanism for active Cl^- extrusion because, in its absence, the conductive Cl^- loads generated during neuronal activity (Buzsáki et al., 2007) would lead to a progressive depolarizing E_{GABA} shift, eventually giving rise to pathophysiological manifestations (see, e.g., Nardou et al., 2011).

Here, we demonstrate a robust enhancement of GDPs by the KCC2 inhibitor VU0463271 (Delpire et al., 2012; Sivakumaran et al., 2015) in neonatal rats and wild-type mice as early as embryonic day (E) 17.5. Importantly, VU0463271 did not affect GDPs in $KCC2^{-/-}$ littermates. VU0463271 increased the spiking rates of CA3 pyramidal neurons, but not of the interneurons targeting these pacemaker cells. Somatic whole-cell Cl^- loading experiments revealed the ability of perinatal CA3 pyramidal neurons to actively extrude Cl^- in a KCC2-dependent manner. Pharmacological inhibition of KCC2 enhanced the depolarizing GABAergic synaptic drive onto neonatal CA3 pyramidal neurons, as seen in gramicidin-perforated patch recordings, and increased their synchronous firing during the rising phase of a GDP. Our data demonstrate that KCC2 has an important role in restraining GDPs already at their developmental onset.

RESULTS

KCC2 Modulates GDPs in the Perinatal Hippocampus

GDPs first appear in the mouse and rat hippocampus perinatally (Khazipov et al., 2004; Crépel et al., 2007; Spoljaric

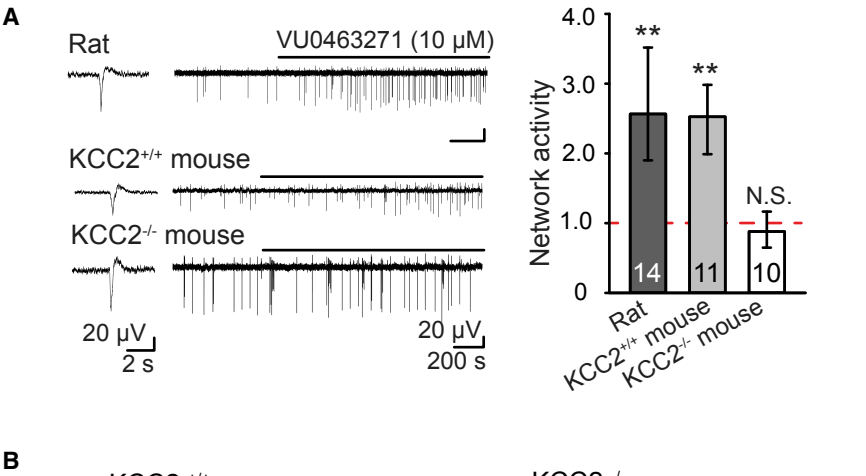

Figure 1. KCC2 Modulates GDPs in the Perinatal Rodent Hippocampus

(A) Effect of the specific KCC2 inhibitor VU0463271 (10 μM) on GDPs in the perinatal rat (P0–P2) and mouse (E17.5–E18.5) hippocampal CA3 area. From left to right: magnified example events from rat, $KCC2^{+/+}$, and $KCC2^{-/-}$ mouse local field potential (LFP) recordings (filtered 1–10 Hz); sample LFP traces (filtered 1–10 Hz); and quantification of normalized network activity after application of VU0463271 are shown. Data are presented as median and IQR; Wilcoxon signed-rank test was used for statistical analysis; **$p < 0.01$; N.S., non-significant; *n* values are indicated in the bar diagram.

(B) KCC2 expression in E18.5 mouse hippocampal CA3 area of $KCC2^{+/+}$ and $KCC2^{-/-}$ mice. In both panels, the areas indicated with rectangles (left) are shown as magnified insets (right). Examples of KCC2-expressing cells are indicated with stars. See also Figures S1, S2, and S3.

et al., 2017). To study the possible role of KCC2 in the modulation of GDPs around their developmental onset, we used E17.5–E18.5 mice and P0–P2 rats, which are at a similar level of cortical development (Clancy et al., 2001; Li et al., 2002). P5 rats served as a positive control, as this is the earliest time point when functionally significant levels of transport-active KCC2 have thus far been reported to be present in the rat hippocampus (Khirug et al., 2010). In P5 rat hippocampal slices, the KCC2 inhibitor VU0463271 (10 μM) induced a sustained increase (fold change 2.44; interquartile range [IQR] 1.80–3.93; n = 7; p = 0.018; Figure S1) in the total area of the local field potential (LFP) events as a function of time, which takes into account the changes in both frequency and amplitude of the events (Spoljaric et al., 2017). Strikingly, VU0463271 induced a similarly robust, sustained increase (fold change: 2.57; IQR 1.90–3.52; n = 14; p = 0.001; Figure 1A) in slices from P0–P2 rats. GDPs recorded in the presence of VU0463271 were fully blocked by the NKCC1 inhibitor bumetanide (10 μM) at all ages studied (n = 11; Figure S2), indicating that the network events recorded in the presence of VU0463271 are dependent on depolarizing GABA.

In line with a previous report (Khalilov et al., 2011) and the above pharmacological data, genetic ablation of KCC2, as seen in intact hippocampi prepared from E17.5–E18.5 $KCC2^{-/-}$ mice, resulted in a marked increase in median GDP amplitude, which was significantly higher in $KCC2^{-/-}$ mice compared to $KCC2^{+/+}$ littermates (50.7 μV [IQR 42.8–77.8 μV] in $KCC2^{-/-}$ [n = 10] versus 33.4 μV [IQR 23.1–52.7 μV] in $KCC2^{+/+}$ [n = 11]; p = 0.008; Mann-Whitney U test; see sample traces in Figure 1A).

No difference was observed in the median frequency of GDPs between the two genotypes (0.0096 Hz [IQR 0.0048–0.016 Hz] in $KCC2^{-/-}$ [n = 10] versus 0.0075 Hz [IQR 0.0058–0.0208 Hz] in $KCC2^{+/+}$ [n = 11]; p = 0.512; Mann-Whitney U test). Immunohistochemical analysis verified KCC2 expression in the CA3 area of E18.5 mouse hippocampi (Figure 1B; see also Khalilov et al., 2011).

Although significant improvement in the specificity of the KCC2 inhibitor VU0463271 (Delpire et al., 2012; Sivakumaran et al., 2015) has been achieved with regard to the potency and ancillary pharmacology of the non-selective parent compound VU0240551 (Delpire et al., 2009), no knockout validation of VU0463271 has thus far been performed. To test whether the enhancement of GDPs by VU0463271 is indeed mediated by specific inhibition of KCC2, we used intact hippocampi from E17.5–E18.5 $KCC2^{-/-}$ and $KCC2^{+/+}$ embryos. In line with the idea that VU0463271 exerts its action by inhibition of KCC2, GDP activity was markedly increased by the drug in $KCC2^{+/+}$ (fold change: 2.53; IQR 1.99–2.98; n = 11; p = 0.003), but not in $KCC2^{-/-}$ mice (fold change: 0.88; IQR 0.65–1.17; n = 10; p = 0.285; Figure 1A; see also Figure S3). As shown previously by Khalilov et al., 2011 using bicuculline, GDPs were abolished by blockade of $GABA_A$Rs with picrotoxin (100 μM) in both $KCC2^{+/+}$ and $KCC2^{-/-}$ hippocampi (n = 6, each genotype; data not shown).

Inhibition of KCC2 Increases GABA-Driven Spontaneous Spiking of Pyramidal Neurons

Because both principal cells and GABAergic interneurons are recruited during GDPs (Sipilä et al., 2005; Ben-Ari et al., 2007; Picardo et al., 2011), changes in the activity of either or both cell types could explain the enhancement of GDPs induced by VU0463271. KCC2 immunohistochemistry in perinatal GAD67-GFP mice suggested that the majority of cells in the CA3 area

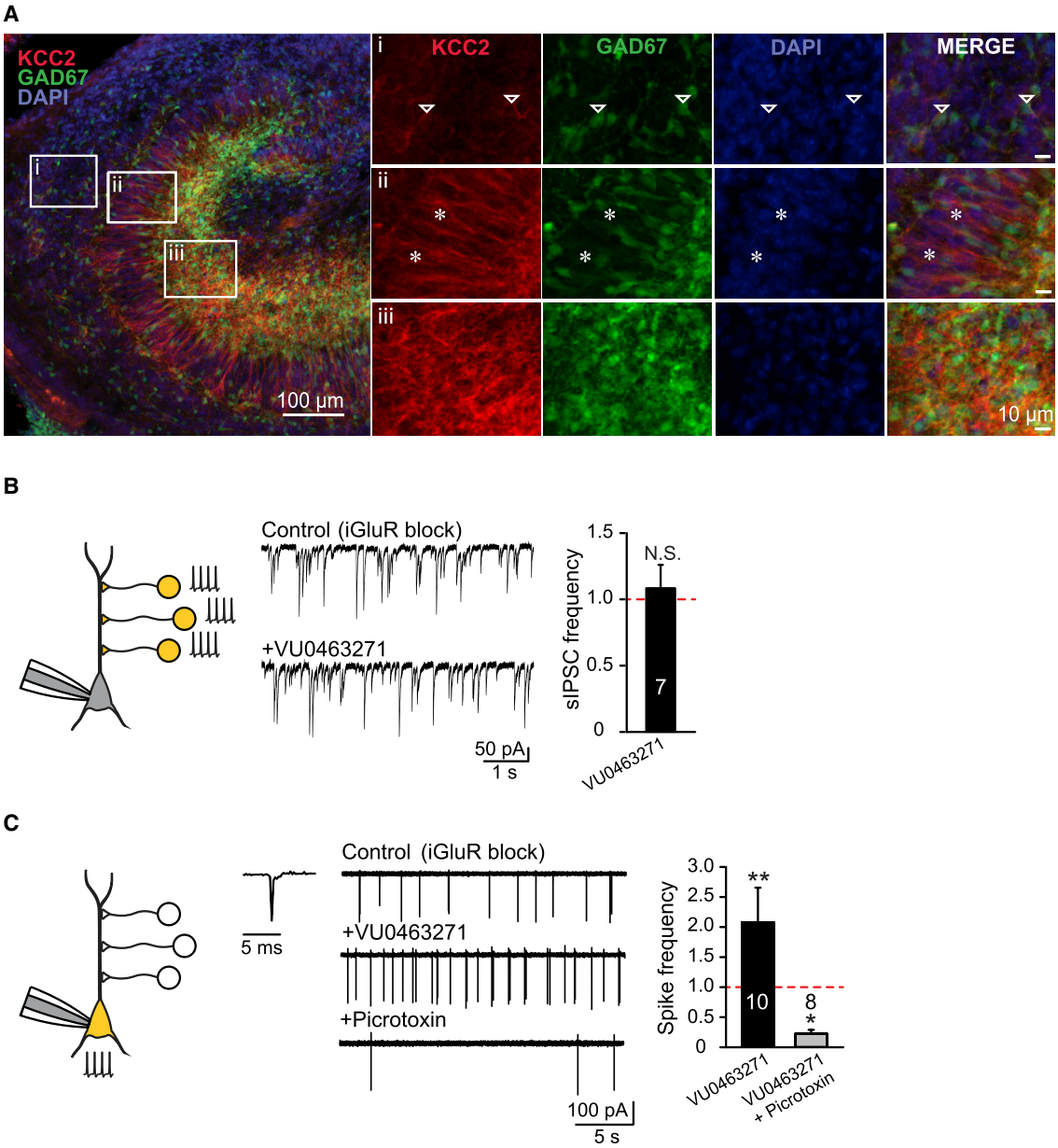

Figure 2. Inhibition of KCC2 Increases GABA-Driven Spontaneous Spiking in CA3 Pyramidal Neurons, but Not in Interneurons

(A) KCC2 expression in E18.5 GAD67-GFP mouse hippocampal CA3 area. The areas indicated with rectangles (left) are shown in more detail on the right. Examples of KCC2-expressing interneurons and pyramidal neurons are indicated with arrowheads and stars, respectively.

(B) Scheme of experimental paradigm to record interneuronal activity from a pyramidal neuron (left). Sample traces of a whole-cell voltage-clamp recording (middle) and median of the normalized frequency values (right) of sIPSCs recorded from pyramidal neurons before and after the application of VU0463271 (10 μM) are shown.

(C) Scheme of experimental paradigm to record pyramidal neuron activity in loose cell-attached configuration (left). Sample traces of a loose cell-attached recording of CA3 pyramidal neuron spiking (middle) and median of the normalized spike frequency (right) in the presence and absence of VU0463271 and picrotoxin (100 μM) are shown. Recordings in (B) and (C) were done in the presence of CNQX (10 μM) and D-AP5 (20 μM), indicated in the figure as iGluR block. Data are presented as median and IQR; Wilcoxon signed-rank test was used for statistical analysis; *$p < 0.05$; **$p < 0.01$; n values are indicated in the bar diagrams.

with distinct KCC2 expression were non-GABAergic (Figure 2A). Analysis of KCC2 immunoreactivity in E18.5–P1 mouse CA3 showed that a total of 89 of 290 principal neurons and 48 of 300 interneuron somata were KCC2 positive (pooled data from 17 slices). When evaluating data of this kind in a functional context, it should be noted that KCC2 molecules may reside in a kinetically inactive state (Rinehart et al., 2009; Khirug et al., 2010) or serve ion-transport-independent functions (Kaila et al.,

2014). Furthermore, the data above does not take into account KCC2 expressed in the distal dendritic compartments of pyramidal neurons (Gulyás et al., 2001). To shed light on the KCC2 pool involved in modulation of GDPs, we differentially examined the effect of VU0463271 on pyramidal cells and those interneurons that are synaptically coupled to CA3 pyramidal neurons in the slice. To this end, we assessed the effects of VU0463271 in loose cell-attached recordings of pyramidal spiking and in whole-cell recordings of spontaneous inhibitory postsynaptic currents (sIPSCs) from P0–P2 rat CA3 pyramidal neurons in the presence of ionotropic glutamate receptor blockers (iGluR block: CNQX 10 μM, D-AP5 20 μM). VU0463271 induced no changes in sIPSC frequency (fold change: 0.91; IQR 0.85–1.09; n = 7; p = 0.499; Figure 2B), whereas it increased the spontaneous spiking of pyramidal neurons (Friedman's test; p = 0.001; fold change: 1.36; IQR 1.23–2.21; n = 10; p = 0.007; Figure 2C). The $GABA_AR$ antagonist picrotoxin suppressed the spontaneous spiking of pyramidal neurons in the presence of VU0463271 and iGluR blockers (fold change compared to control: 0.22; IQR 0.07–0.34; n = 8; p = 0.012; Figure 2C), suggesting that the effect of VU0463271 is due to changes in the driving force of $GABA_AR$-mediated currents.

VU0463271-Sensitive Chloride Extrusion in Neonatal CA3 Pyramidal Neurons

Previous work, employing gramicidin-perforated patch recordings, showed no difference in somatic steady-state E_{GABA} between $KCC2^{+/+}$ and $KCC2^{-/-}$ mouse CA3 pyramidal neurons at E18.5 (Khalilov et al., 2011). Such data, obtained under conditions with no constant Cl^- load, revealed a vast cell-to-cell heterogeneity in the intracellular somatic Cl^- levels (see also Lombardi et al., 2018). This variation may reflect differences in the functional expression levels of both Cl^- importing and extruding proteins. Using a somatic Cl^- loading technique (Khirug et al., 2005; Li et al., 2007; Puskarjov et al., 2015, 2017), we found previously that E_{GABA} levels of $GABA_AR$-mediated currents recorded in the presence of the NKCC1 inhibitor bumetanide and evoked at 50–100 μm from the soma of hippocampal neurons reflect a steep increase in KCC2-mediated Cl^- extrusion during the first two weeks of postnatal development in mouse and rat (Khirug et al., 2005; Spoljaric et al., 2017). Under a defined somatically imposed Cl^- load and NKCC1 block, we observed in P1 rat CA3 pyramidal neurons a negligible deviation of the E_{GABA}, determined using GABA uncaging, from the calculated passive Cl^- distribution ($E_{GABA\text{-}GHK}$; see STAR Methods) at the soma ($\Delta E_{GABA} = E_{GABA} - E_{GABA\text{-}GHK} = -0.8$ mV; IQR −1.2 to −0.4 mV) and at a distance of 50 μm in the apical dendrite ($\Delta E_{GABA} = -3.1$ mV; IQR −3.7 to −2.4 mV; n = 4 each; Figures 3A and 3B). This level of the ΔE_{GABA} recorded at 50 μm from the soma of P1 CA3 pyramids is, in fact, similar to that recorded in more mature hippocampal and neocortical pyramidal neurons following pharmacological block of K-Cl cotransport (Spoljaric et al., 2017) or genetic deletion of KCC2 (Li et al., 2007; Puskarjov et al., 2017). In contrast, and as expected in light of the developmental upregulation of KCC2 during the first two weeks of rat hippocampal postnatal development (Khirug et al., 2005; Spoljaric et al., 2017), a large negative shift in dendritic E_{GABA} at 50 μm was observed in P17 CA3 pyramidal neurons (ΔE_{GABA} = −9.9 mV; IQR −11.7 to −9.7 mV; p = 0.02 compared to P1; Mann-Whitney U test; not illustrated), and somatic E_{GABA} was still close to $E_{GABA\text{-}GHK}$ ($\Delta E_{GABA} = -2.0$ mV; IQR −2.1 to −1.5 mV; n = 5 each; not illustrated). To examine whether a significant level of KCC2-mediated K-Cl cotransport can be detected in the perinatal CA3 pyramidal neurons, we improved the sensitivity of our Cl^- extrusion assay by recording dendritic E_{GABA} values at a larger distance, 200 μm, from the soma (Figures 3A–3C). This approach uncovered the presence of KCC2-mediated Cl^- extrusion in CA3 pyramids at P1 as indicated by the VU0463271-mediated positive shift in ΔE_{GABA} (Ctrl: $\Delta E_{GABA} = -11.3$ mV [IQR −16.9 to −9.9 mV]; VU0463271: $\Delta E_{GABA} = -6.3$ mV [IQR −6.6 to −3.5 mV]; n = 5; p = 0.04; Figures 3B and 3C). These data demonstrate that neonatal CA3 pyramidal neurons are able to actively extrude Cl^- in a KCC2-dependent manner in the dendrites below the level set by passive distribution. Obviously, this does not exclude the presence of Cl^- extrusion mechanisms in the somatic compartment. Moreover, the above approach based on exogenous (uncaged) GABA does not provide information on whether the observed Cl^- extrusion occurs at GABAergic synapses. To investigate how pharmacological inhibition of KCC2 affects the driving force of synaptic $GABA_AR$-mediated currents (DF_{GABA}) under conditions of otherwise unperturbed Cl^- homeostasis, we performed gramicidin-perforated patch recordings of miniature inhibitory postsynaptic currents (mIPSCs) at resting membrane potential in the absence of bumetanide. These experiments demonstrated a VU0463271-induced increase in mIPSC amplitude (fold change: 1.50; IQR 1.15–2.04; p = 0.018; Figure 3D), which was not seen in the controls (amplitude fold change: 1.10; IQR 0.79–1.19; p = 0.5; Figure 3D). The above results demonstrate an enhanced depolarizing synaptic GABAergic drive after selective pharmacological inhibition of KCC2.

Inhibition of KCC2 Shifts the Spike Distribution of CA3 Pyramidal Neurons toward the Rising Phase of GDPs

GDPs act to synchronize neuronal firing in the CA3 pyramidal cell layer (Khalilov et al., 2015). After establishing that VU0463271 increases DF_{GABA} (Figure 3) and the GABA-driven spontaneous spiking of CA3 pyramidal neurons (Figure 2), we examined the effects of KCC2 inhibition on GDP-nested spiking of the CA3 pyramidal neurons. Because the depolarizing GABAergic drive is crucial in shaping GDPs (Ben-Ari et al., 1989; Sipilä et al., 2005; Valeeva et al., 2013; Spoljaric et al., 2017), inhibition of KCC2 is expected to increase the network-level synchronization of pyramidal neurons (see below). In simultaneous loose cell-attached and multi-unit activity (MUA) recordings of CA3 pyramidal neuron spiking, the overall number of GDP-nested spikes did not change significantly during VU0463271 application (loose cell-attached, fold change: 1.16 [IQR 0.97–1.4], n = 6, p = 0.16; MUA, fold change: 0.77 [IQR 0.7–1.12], n = 6, p = 0.44; Figures 4A and 4D). However, the relative number of spikes during the rising phase of GDPs in comparison to the total number of GDP-nested spikes was significantly increased during VU0463271 application in both loose cell-attached and MUA recordings (loose cell-attached, control: 0.36 [IQR 0.14–0.56] versus VU0463271: 0.48 [IQR 0.33–0.69], n = 6, p = 0.031;

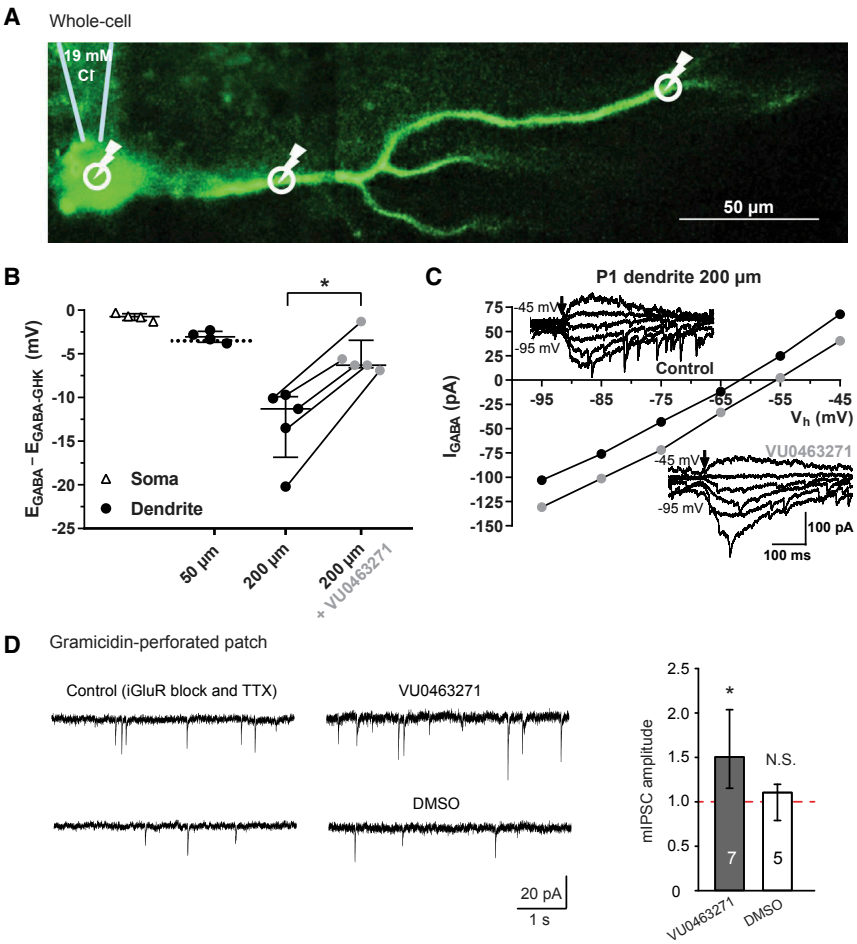

Figure 3. VU0463271-Sensitive Chloride Extrusion in Neonatal CA3 Pyramidal Neurons

(A) An Alexa Fluor 488-filled CA3 pyramidal neuron from a P1 rat representing the position of the whole-cell patch pipette imposing a 19 mM Cl^- load onto the neuron and the sites of UV photolysis of caged GABA.

(B) Chloride extrusion efficacy in P1 rat CA3 pyramidal neurons determined using local UV photolysis of caged GABA at the soma (n = 4) and apical dendrite at 50 µm (n = 4) and 200 µm (n = 5) distance from the somatic Cl^- load, under control conditions (black) and in the presence of VU0463271 (10 µM, gray). Stippled line delimits the approximate residual negative deflection in E_{GABA} from $E_{GABA-GHK}$ at 50 µm that is insensitive to VU0463271 (see Spoljaric et al., 2017) and present in $KCC2^{-/-}$ neurons (see Li et al., 2007).

(C) Sample E_{GABA} recordings and their corresponding I-V plots in the presence of iGluR block and bumetanide (2.5 µM).

(D) Sample traces of gramicidin-perforated patch recordings (left) and median of the normalized amplitude of miniature inhibitory postsynaptic currents (mIPSCs; right) recorded from pyramidal neurons before and after the application of VU0463271 or DMSO. Recordings were done in the presence of iGluR block and TTX (0.5 µM). Data in (B) and (D) are presented as median and IQR; Wilcoxon signed-rank test were used for statistical analysis; *p < 0.05; n values are indicated in the bar diagram.

MUA, control: 0.30 [IQR 0.24–0.34] versus VU0463271: 0.43 [IQR 0.30–0.60], n = 6, p = 0.031; Figures 4A–4D). This shows that the VU0463271-induced increase in DF_{GABA} leads to increased synchronization of pyramidal neuron spiking during the rising phase of GDPs.

Collectively, our data indicate that KCC2-mediated Cl^- extrusion acts to limit the depolarizing GABAergic drive in the perinatal hippocampus of both rat and mouse, which readily explains the VU0463271-induced increase in spontaneous network activity.

DISCUSSION

The main finding of the present study is that transport-functional KCC2 is expressed at physiologically significant levels in perinatal CA3 pyramidal neurons of rats and mice, i.e., at a surprisingly early stage of hippocampal development. KCC2 mRNA has been observed in the mouse CA3 as early as E15.5 (Stein et al., 2004), and work on E18.5 mouse embryos reported a modest level of KCC2 immunoreactivity in CA3 pyramidal neurons (Khalilov et al., 2011). The role of this early KCC2 expression has remained poorly defined. In the present work, we found that KCC2 has an important role in restraining GDPs in neonatal mice and rats by opposing Cl^- uptake via NKCC1, which at this developmental stage is dominant and maintains $GABA_AR$-mediated currents strongly depolarizing (Sipilä et al., 2006, 2009; Pfeffer et al., 2009; Khazipov et al., 2015; Spoljaric et al., 2017). In P0–P2 rat hippocampal slices, inhibition of KCC2 increased spontaneous spiking of CA3 pyramidal neurons as well as their synchrony during the rising phase of a GDP, with no significant effect on the number of GDP-nested spikes. In agreement with the idea that KCC2 acts to suppress GDP activity, we observed that these events had a higher amplitude in KCC2-null versus wild-type animals, and this difference was closely mimicked by exposure of wild-type mouse hippocampi to the KCC2 blocker VU0463271. Based on our data on $KCC2^{+/+}$ versus $KCC2^{-/-}$ mouse embryos, VU0463271 used at 10 µM shows a high level of specificity, because it does not seem to have off-target effects on the multiple molecular mechanisms that are involved in the generation of GDPs (Ben-Ari et al., 2007; Griguoli and Cherubini, 2017).

We found using whole-cell recordings that rat neonatal CA3 pyramidal neurons are equipped with a sufficient amount of functional KCC2 to counteract a constant experimentally imposed Cl^- load. Furthermore, using gramicidin-perforated patch recordings, we demonstrated that KCC2 expressed at this age in CA3 pyramids maintains a less depolarizing driving force of synaptic $GABA_AR$-mediated currents than the one observed in its absence.

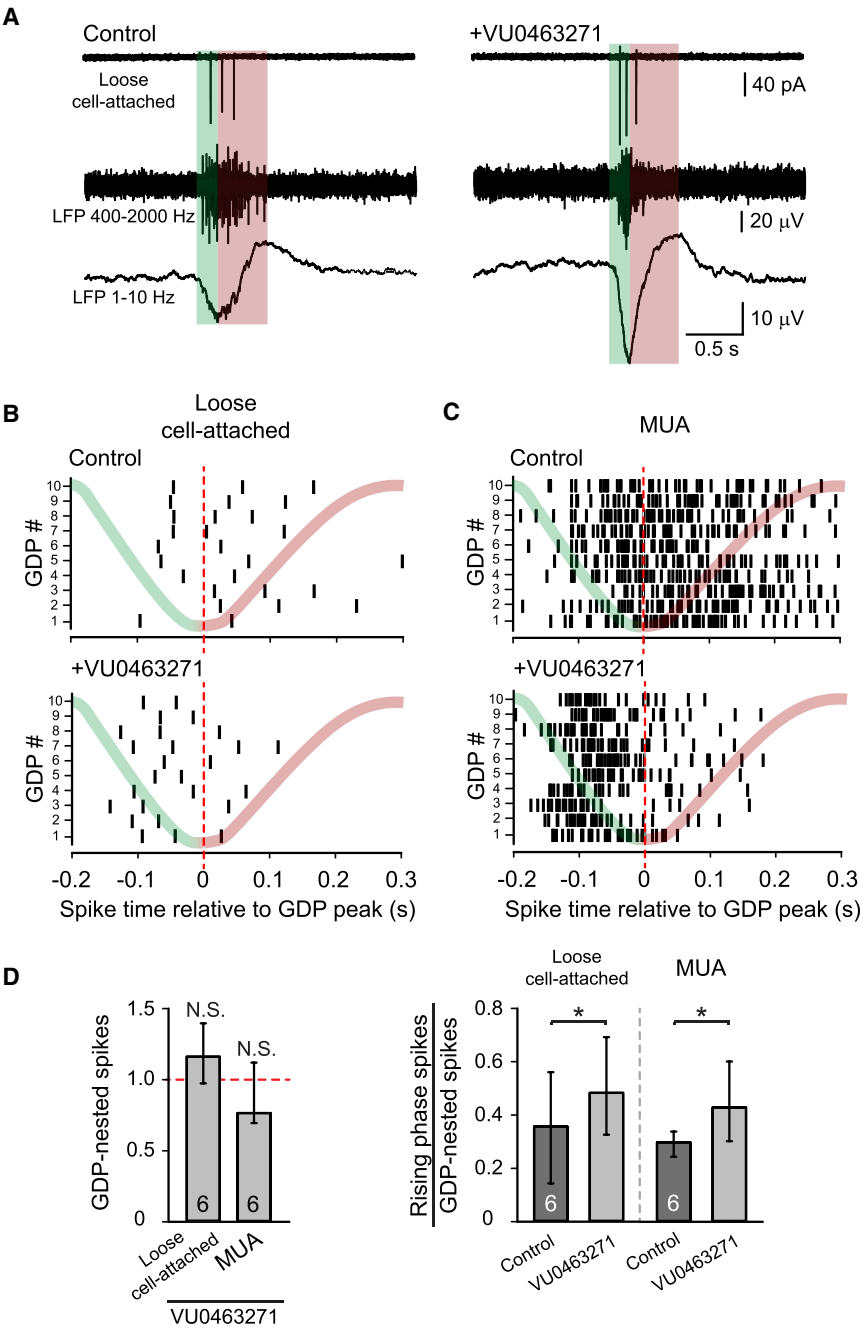

Figure 4. Inhibition of KCC2 Shifts the Spike Distribution of CA3 Pyramidal Neurons toward the Rising Phase of GDPs

(A) Sample traces from simultaneous loose cell-attached (top) and local field potential (LFP) recordings (middle: multi-unit activity [MUA], bandpass 400-2000 Hz; bottom: GDP, bandpass 1-10 Hz) of CA3 pyramidal neuron spiking in the absence and presence of VU0463271 (10 μM). The colored boxes over the sample traces highlight the rising phase (green) and falling phase (red) of the GDP.

(B and C) Example raster plots of CA3 pyramidal neuron spiking during 10 control GDPs and 10 GDPs during VU0463271 application from a simultaneous loose cell-attached recording of spiking (B) and LFP recording of MUA (C). The peak of the GDPs is set to time point 0 s. The mock GDP shape in the background of the raster plots portrays the rising and falling phases of the GDPs.

(D) Median values of normalized GDP-nested spikes in both loose cell-attached and MUA recordings during VU0463271 (left). Number of spikes observed in loose cell-attached and MUA recordings during the rising phase of GDPs, in relation to the total number of GDP-nested spikes, in the absence and presence of VU0463171 (right) is shown. Data are presented as median and IQR; Wilcoxon signed-rank test was used for statistical analysis; *$p < 0.05$; n values are indicated in the bar diagrams.

Recent work on neonatal rat CA3 pyramidal neurons suggests that GABAergic actions change dynamically from depolarizing to hyperpolarizing during GDPs, which is thought to prevent epileptiform synchronization in the recurrent CA3 network (Khalilov et al., 2015). According to this scheme, at the onset of a GDP, the excitatory inward current is driven by depolarizing NKCC1-dependent $GABA_A$R-mediated and by glutamatergic synaptic currents as shown in a number of studies (reviewed by Ben-Ari et al., 2007). However, at the peak of a GDP, when the momentary membrane potential is depolarized beyond E_{GABA}, I_{GABA} transiently switches its polarity (Khalilov et al., 2015) to become an outward current enabling effective shunting (see Kaila et al., 2014) of the glutamatergic input via simultaneously open $GABA_A$Rs (Khalilov et al., 2015). In the absence of active Cl^- extrusion, conductive Cl^- loading during neuronal network activity would lead to a progressive, uncontrolled depolarizing E_{GABA} shift (Kaila et al., 2014) and, consequently, to epileptiform activity. Indeed, downregulation of KCC2 in an *in vitro* model of neonatal seizures has been shown to result in accumulation of intracellular Cl^-, thereby contributing to the aggravation of epileptiform activity by phenobarbital (Nardou et al., 2011).

Although we found that the KCC2 inhibitor VU0463271 increased the firing rate of P0–P2 rat hippocampal CA3 pyramidal neurons in the absence of glutamatergic transmission, we observed no change in the output of interneurons synapsing onto pyramidal neurons. Immature pyramidal neurons have been reported to receive GABAergic innervation predominantly onto their dendrites (Tyzio et al., 1999; Khazipov et al., 2001; Morozov and Freund, 2003). Indeed, CA3 pyramidal dendrites were presently found to be equipped with transport-functional KCC2 at a level sufficient to oppose a significant Cl^- load. Hippocampal interneurons constitute a developmentally and functionally heterogeneous cell

population and, not surprisingly, diverse actions of GABA on neonatal interneurons have been reported (Leinekugel et al., 1995; Khazipov et al., 1997; Bolea et al., 1999; Verheugen et al., 1999; Banke and McBain, 2006; Tyzio et al., 2008; Sauer and Bartos, 2010). Recent work on early-born GABAergic hub neurons—a subpopulation of CA3 interneurons critical for regulation of hippocampal spontaneous network events (Bonifazi et al., 2009; Picardo et al., 2011)—reported no expression of KCC2 between E18.5 and P1, and at P2–P4, less than ten percent of them are KCC2 positive (Villette et al., 2016). In embryonic mouse neocortical explants grown *in vitro*, KCC2 expression has been reported to be predominantly interneuronal (Bortone and Polleux, 2009). The above is apparently not the case for the perinatal hippocampal CA3 area *ex vivo*, where higher KCC2 expression was observed in the pyramidal neurons than in interneurons.

In studies on perinatal rats and mice, which are by far the most widely used animals in biomedical research, it is sometimes overlooked that the level of brain maturation at birth shows extensive variation among mammalian species—a point which has a profound relevance on translational studies on brain development and its disorders. Indeed, observations on a precocial species, the macaque, have demonstrated GABAergic inhibition by blocking $GABA_A$Rs in the hippocampus *ex utero* during the last trimester of gestation (Khazipov et al., 2001). In contrast to primates and the guinea pig, which have high levels of KCC2 in cortical neurons much before birth (Rivera et al., 1999; Vanhatalo et al., 2005; Sedmak et al., 2016; Spoljaric et al., 2017), rats and mice are both altricial rodents, i.e., are born at a very immature stage of cortical development, which corresponds to human postconceptional weeks (PCWs) 25–27 (Clancy et al., 2001). In the human cortex, strong developmental upregulation of KCC2 mRNA takes place between the beginning of the third trimester and approximately the third postnatal month (Vanhatalo et al., 2005; Sedmak et al., 2016), and at PCW 25, most human cortical neurons express KCC2 protein (Sedmak et al., 2016). When setting our data into the context of this cross-species calibration of developmental age, aberrations in cortical KCC2 functions, such as those caused by epilepsy mutations (Puskarjov et al., 2014; Kahle et al., 2014; Stödberg et al., 2015; Saito et al., 2017), are likely to interfere with activity-dependent neuronal wiring within a prolonged (~15 weeks) prenatal time window in humans. In addition to compromised neuronal Cl^- extrusion as such, it is also possible that the development of the epilepsy phenotype has at least some of its roots in aberrant prenatal GDPs as demonstrated by Khalilov et al. (2011), with consequent disturbances in the development of the hippocampal circuitry (see Introduction).

In summary, our study shows that functional KCC2 is expressed at a surprisingly early developmental stage in the CA3 region of the hippocampus, where it exerts a significant restraining influence on CA3-driven network events, the GDPs. An interesting question for future research is whether the presence of transport-functional KCC2 is tightly involved in the ontogeny of multiregional spontaneous activity patterns, analogous to GDPs (Ben-Ari et al., 2007; Blankenship and Feller, 2010).

STAR★METHODS

Detailed methods are provided in the online version of this paper and include the following:

- KEY RESOURCES TABLE
- CONTACT FOR REAGENT AND RESOURCE SHARING
- EXPERIMENTAL MODEL AND SUBJECT DETAILS
- METHOD DETAILS
  - Hippocampal preparations
  - Electrophysiological recordings
  - Analysis of electrophysiological recordings
  - Immunohistochemistry
- QUANTIFICATION AND STATISTICAL ANALYSIS

SUPPLEMENTAL INFORMATION

Supplemental Information includes three figures and can be found with this article online at https://doi.org/10.1016/j.celrep.2019.01.011.

ACKNOWLEDGMENTS

We thank Merle Kampura and Maria Partanen for excellent technical assistance and breeding of the animals and Prof. Juha Voipio and Drs. Eva Ruusuvuori and Mari Virtanen for comments on the manuscript. This work was supported by grants from the Academy of Finland (to K.K.), European Research Council (grant ERC-2013-AdG 341116 to K.K.), and the Emil Aaltonen Foundation (to M.P.). K.K. ORCID ID: 0000-0003-0668-5955.

AUTHOR CONTRIBUTIONS

I.S., A.S., M.M., P.S., and M.P. performed the experiments and analyzed the data; I.S., A.S., P.S., M.P., and K.K. designed the experiments; M.P. and K.K. directed the study; and I.S., M.P., and K.K. wrote the manuscript.

DECLARATION OF INTERESTS

The authors declare no competing interests.

Received: July 24, 2018
Revised: November 30, 2018
Accepted: January 2, 2019
Published: January 29, 2019

REFERENCES

Banke, T.G., and McBain, C.J. (2006). GABAergic input onto CA3 hippocampal interneurons remains shunting throughout development. J. Neurosci. *26*, 11720–11725.

Ben-Ari, Y., Cherubini, E., Corradetti, R., and Gaiarsa, J.L. (1989). Giant synaptic potentials in immature rat CA3 hippocampal neurones. J. Physiol. *416*, 303–325.

Ben-Ari, Y., Gaiarsa, J.L., Tyzio, R., and Khazipov, R. (2007). GABA: a pioneer transmitter that excites immature neurons and generates primitive oscillations. Physiol. Rev. *87*, 1215–1284.

Blankenship, A.G., and Feller, M.B. (2010). Mechanisms underlying spontaneous patterned activity in developing neural circuits. Nat. Rev. Neurosci. *11*, 18–29.

Bolea, S., Avignone, E., Berretta, N., Sanchez-Andres, J.V., and Cherubini, E. (1999). Glutamate controls the induction of GABA-mediated giant depolarizing potentials through AMPA receptors in neonatal rat hippocampal slices. J. Neurophysiol. *81*, 2095–2102.

Bonifazi, P., Goldin, M., Picardo, M.A., Jorquera, I., Cattani, A., Bianconi, G., Represa, A., Ben-Ari, Y., and Cossart, R. (2009). GABAergic hub neurons

orchestrate synchrony in developing hippocampal networks. Science *326*, 1419–1424.

Bortone, D., and Polleux, F. (2009). KCC2 expression promotes the termination of cortical interneuron migration in a voltage-sensitive calcium-dependent manner. Neuron *62*, 53–71.

Buzsáki, G., Kaila, K., and Raichle, M. (2007). Inhibition and brain work. Neuron *56*, 771–783.

Chamma, I., Heubl, M., Chevy, Q., Renner, M., Moutkine, I., Eugène, E., Poncer, J.C., and Lévi, S. (2013). Activity-dependent regulation of the K/Cl transporter KCC2 membrane diffusion, clustering, and function in hippocampal neurons. J. Neurosci. *33*, 15488–15503.

Clancy, B., Darlington, R.B., and Finlay, B.L. (2001). Translating developmental time across mammalian species. Neuroscience *105*, 7–17.

Crépel, V., Aronov, D., Jorquera, I., Represa, A., Ben-Ari, Y., and Cossart, R. (2007). A parturition-associated nonsynaptic coherent activity pattern in the developing hippocampus. Neuron *54*, 105–120.

Delpire, E., Days, E., Lewis, L.M., Mi, D., Kim, K., Lindsley, C.W., and Weaver, C.D. (2009). Small-molecule screen identifies inhibitors of the neuronal K-Cl cotransporter KCC2. Proc. Natl. Acad. Sci. USA *106*, 5383–5388.

Delpire, E., Baranczak, A., Waterson, A.G., Kim, K., Kett, N., Morrison, R.D., Daniels, J.S., Weaver, C.D., and Lindsley, C.W. (2012). Further optimization of the K-Cl cotransporter KCC2 antagonist ML077: development of a highly selective and more potent in vitro probe. Bioorg. Med. Chem. Lett. *22*, 4532–4535.

Dzhala, V.I., Talos, D.M., Sdrulla, D.A., Brumback, A.C., Mathews, G.C., Benke, T.A., Delpire, E., Jensen, F.E., and Staley, K.J. (2005). NKCC1 transporter facilitates seizures in the developing brain. Nat. Med. *11*, 1205–1213.

Griguoli, M., and Cherubini, E. (2017). Early correlated network activity in the hippocampus: its putative role in shaping neuronal circuits. Front. Cell. Neurosci. *11*, 255.

Gulyás, A.I., Sík, A., Payne, J.A., Kaila, K., and Freund, T.F. (2001). The KCl cotransporter, KCC2, is highly expressed in the vicinity of excitatory synapses in the rat hippocampus. Eur. J. Neurosci. *13*, 2205–2217.

Hübner, C.A., Stein, V., Hermans-Borgmeyer, I., Meyer, T., Ballanyi, K., and Jentsch, T.J. (2001). Disruption of KCC2 reveals an essential role of K-Cl cotransport already in early synaptic inhibition. Neuron *30*, 515–524.

Kahle, K.T., Merner, N.D., Friedel, P., Silayeva, L., Liang, B., Khanna, A., Shang, Y., Lachance-Touchette, P., Bourassa, C., Levert, A., et al. (2014). Genetically encoded impairment of neuronal KCC2 cotransporter function in human idiopathic generalized epilepsy. EMBO Rep. *15*, 766–774.

Kaila, K., Price, T.J., Payne, J.A., Puskarjov, M., and Voipio, J. (2014). Cation-chloride cotransporters in neuronal development, plasticity and disease. Nat. Rev. Neurosci. *15*, 637–654.

Khalilov, I., Esclapez, M., Medina, I., Aggoun, D., Lamsa, K., Leinekugel, X., Khazipov, R., and Ben-Ari, Y. (1997a). A novel in vitro preparation: the intact hippocampal formation. Neuron *19*, 743–749.

Khalilov, I., Khazipov, R., Esclapez, M., and Ben-Ari, Y. (1997b). Bicuculline induces ictal seizures in the intact hippocampus recorded in vitro. Eur. J. Pharmacol. *319*, R5–R6.

Khalilov, I., Dzhala, V., Ben-Ari, Y., and Khazipov, R. (1999). Dual role of GABA in the neonatal rat hippocampus. Dev. Neurosci. *21*, 310–319.

Khalilov, I., Chazal, G., Chudotvorova, I., Pellegrino, C., Corby, S., Ferrand, N., Gubkina, O., Nardou, R., Tyzio, R., Yamamoto, S., et al. (2011). Enhanced synaptic activity and epileptiform events in the embryonic KCC2 deficient hippocampus. Front. Cell. Neurosci. *5*, 23.

Khalilov, I., Minlebaev, M., Mukhtarov, M., and Khazipov, R. (2015). Dynamic changes from depolarizing to hyperpolarizing GABAergic actions during giant depolarizing potentials in the neonatal rat hippocampus. J. Neurosci. *35*, 12635–12642.

Khazipov, R., Leinekugel, X., Khalilov, I., Gaiarsa, J.L., and Ben-Ari, Y. (1997). Synchronization of GABAergic interneuronal network in CA3 subfield of neonatal rat hippocampal slices. J. Physiol. *498*, 763–772.

Khazipov, R., Esclapez, M., Caillard, O., Bernard, C., Khalilov, I., Tyzio, R., Hirsch, J., Dzhala, V., Berger, B., and Ben-Ari, Y. (2001). Early development of neuronal activity in the primate hippocampus in utero. J. Neurosci. *21*, 9770–9781.

Khazipov, R., Khalilov, I., Tyzio, R., Morozova, E., Ben-Ari, Y., and Holmes, G.L. (2004). Developmental changes in GABAergic actions and seizure susceptibility in the rat hippocampus. Eur. J. Neurosci. *19*, 590–600.

Khazipov, R., Valeeva, G., and Khalilov, I. (2015). Depolarizing GABA and developmental epilepsies. CNS Neurosci. Ther. *21*, 83–91.

Khirug, S., Huttu, K., Ludwig, A., Smirnov, S., Voipio, J., Rivera, C., Kaila, K., and Khiroug, L. (2005). Distinct properties of functional KCC2 expression in immature mouse hippocampal neurons in culture and in acute slices. Eur. J. Neurosci. *21*, 899–904.

Khirug, S., Ahmad, F., Puskarjov, M., Afzalov, R., Kaila, K., and Blaesse, P. (2010). A single seizure episode leads to rapid functional activation of KCC2 in the neonatal rat hippocampus. J. Neurosci. *30*, 12028–12035.

Kirmse, K., Hübner, C.A., Isbrandt, D., Witte, O.W., and Holthoff, K. (2018). GABAergic transmission during brain development: multiple effects at multiple stages. Neuroscientist *24*, 36–53.

Kyrozis, A., and Reichling, D.B. (1995). Perforated-patch recording with gramicidin avoids artifactual changes in intracellular chloride concentration. J. Neurosci. Methods *57*, 27–35.

Lamsa, K., Palva, J.M., Ruusuvuori, E., Kaila, K., and Taira, T. (2000). Synaptic GABA(A) activation inhibits AMPA-kainate receptor-mediated bursting in the newborn (P0-P2) rat hippocampus. J. Neurophysiol. *83*, 359–366.

Leinekugel, X., Tseeb, V., Ben-Ari, Y., and Bregestovski, P. (1995). Synaptic GABAA activation induces Ca2+ rise in pyramidal cells and interneurons from rat neonatal hippocampal slices. J. Physiol. *487*, 319–329.

Leinekugel, X., Khalilov, I., Ben-Ari, Y., and Khazipov, R. (1998). Giant depolarizing potentials: the septal pole of the hippocampus paces the activity of the developing intact septohippocampal complex in vitro. J. Neurosci. *18*, 6349–6357.

Li, H., Tornberg, J., Kaila, K., Airaksinen, M.S., and Rivera, C. (2002). Patterns of cation-chloride cotransporter expression during embryonic rodent CNS development. Eur. J. Neurosci. *16*, 2358–2370.

Li, H., Khirug, S., Cai, C., Ludwig, A., Blaesse, P., Kolikova, J., Afzalov, R., Coleman, S.K., Lauri, S., Airaksinen, M.S., et al. (2007). KCC2 interacts with the dendritic cytoskeleton to promote spine development. Neuron *56*, 1019–1033.

Lombardi, A., Jedlicka, P., Luhmann, H.J., and Kilb, W. (2018). Giant depolarizing potentials trigger transient changes in the intracellular Cl^- concentration in CA3 pyramidal neurons of the immature mouse hippocampus. Front. Cell. Neurosci. *12*, 420.

Morozov, Y.M., and Freund, T.F. (2003). Postnatal development and migration of cholecystokinin-immunoreactive interneurons in rat hippocampus. Neuroscience *120*, 923–939.

Nardou, R., Yamamoto, S., Chazal, G., Bhar, A., Ferrand, N., Dulac, O., Ben-Ari, Y., and Khalilov, I. (2011). Neuronal chloride accumulation and excitatory GABA underlie aggravation of neonatal epileptiform activities by phenobarbital. Brain *134*, 987–1002.

Pfeffer, C.K., Stein, V., Keating, D.J., Maier, H., Rinke, I., Rudhard, Y., Hentschke, M., Rune, G.M., Jentsch, T.J., and Hübner, C.A. (2009). NKCC1-dependent GABAergic excitation drives synaptic network maturation during early hippocampal development. J. Neurosci. *29*, 3419–3430.

Picardo, M.A., Guigue, P., Bonifazi, P., Batista-Brito, R., Allene, C., Ribas, A., Fishell, G., Baude, A., and Cossart, R. (2011). Pioneer GABA cells comprise a subpopulation of hub neurons in the developing hippocampus. Neuron *71*, 695–709.

Puskarjov, M., Seja, P., Heron, S.E., Williams, T.C., Ahmad, F., Iona, X., Oliver, K.L., Grinton, B.E., Vutskits, L., Scheffer, I.E., et al. (2014). A variant of KCC2 from patients with febrile seizures impairs neuronal Cl- extrusion and dendritic spine formation. EMBO Rep. *15*, 723–729.

Puskarjov, M., Ahmad, F., Khirug, S., Sivakumaran, S., Kaila, K., and Blaesse, P. (2015). BDNF is required for seizure-induced but not developmental

up-regulation of KCC2 in the neonatal hippocampus. Neuropharmacology *88*, 103–109.

Puskarjov, M., Fiumelli, H., Briner, A., Bodogan, T., Demeter, K., Lacoh, C.M., Mavrovic, M., Blaesse, P., Kaila, K., and Vutskits, L. (2017). K-Cl cotransporter 2-mediated Cl- extrusion determines developmental stage-dependent impact of propofol anesthesia on dendritic spines. Anesthesiology *126*, 855–867.

Rinehart, J., Maksimova, Y.D., Tanis, J.E., Stone, K.L., Hodson, C.A., Zhang, J., Risinger, M., Pan, W., Wu, D., Colangelo, C.M., et al. (2009). Sites of regulated phosphorylation that control K-Cl cotransporter activity. Cell *138*, 525–536.

Rivera, C., Voipio, J., Payne, J.A., Ruusuvuori, E., Lahtinen, H., Lamsa, K., Pirvola, U., Saarma, M., and Kaila, K. (1999). The K+/Cl- co-transporter KCC2 renders GABA hyperpolarizing during neuronal maturation. Nature *397*, 251–255.

Saito, T., Ishii, A., Sugai, K., Sasaki, M., and Hirose, S. (2017). A de novo missense mutation in SLC12A5 found in a compound heterozygote patient with epilepsy of infancy with migrating focal seizures. Clin. Genet. *92*, 654–658.

Sauer, J.F., and Bartos, M. (2010). Recruitment of early postnatal parvalbumin-positive hippocampal interneurons by GABAergic excitation. J. Neurosci. *30*, 110–115.

Schindelin, J., Arganda-Carreras, I., Frise, E., Kaynig, V., Longair, M., Pietzsch, T., Preibisch, S., Rueden, C., Saalfeld, S., Schmid, B., et al. (2012). Fiji: an open-source platform for biological-image analysis. Nat. Methods *9*, 676–682.

Sedmak, G., Jovanov-Milošević, N., Puskarjov, M., Ulamec, M., Krušlin, B., Kaila, K., and Judaš, M. (2016). Developmental expression patterns of KCC2 and functionally associated molecules in the human brain. Cereb. Cortex *26*, 4574–4589.

Sipilä, S.T., Huttu, K., Soltesz, I., Voipio, J., and Kaila, K. (2005). Depolarizing GABA acts on intrinsically bursting pyramidal neurons to drive giant depolarizing potentials in the immature hippocampus. J. Neurosci. *25*, 5280–5289.

Sipilä, S.T., Schuchmann, S., Voipio, J., Yamada, J., and Kaila, K. (2006). The cation-chloride cotransporter NKCC1 promotes sharp waves in the neonatal rat hippocampus. J. Physiol. *573*, 765–773.

Sipilä, S.T., Huttu, K., Yamada, J., Afzalov, R., Voipio, J., Blaesse, P., and Kaila, K. (2009). Compensatory enhancement of intrinsic spiking upon NKCC1 disruption in neonatal hippocampus. J. Neurosci. *29*, 6982–6988.

Sivakumaran, S., Cardarelli, R.A., Maguire, J., Kelley, M.R., Silayeva, L., Morrow, D.H., Mukherjee, J., Moore, Y.E., Mather, R.J., Duggan, M.E., et al. (2015). Selective inhibition of KCC2 leads to hyperexcitability and epileptiform discharges in hippocampal slices and in vivo. J. Neurosci. *35*, 8291–8296.

Spoljaric, A., Seja, P., Spoljaric, I., Virtanen, M.A., Lindfors, J., Uvarov, P., Summanen, M., Crow, A.K., Hsueh, B., Puskarjov, M., et al. (2017). Vasopressin excites interneurons to suppress hippocampal network activity across a broad span of brain maturity at birth. Proc. Natl. Acad. Sci. USA *114*, E10819–E10828.

Stein, V., Hermans-Borgmeyer, I., Jentsch, T.J., and Hübner, C.A. (2004). Expression of the KCl cotransporter KCC2 parallels neuronal maturation and the emergence of low intracellular chloride. J. Comp. Neurol. *468*, 57–64.

Stödberg, T., McTague, A., Ruiz, A.J., Hirata, H., Zhen, J., Long, P., Farabella, I., Meyer, E., Kawahara, A., Vassallo, G., et al. (2015). Mutations in *SLC12A5* in epilepsy of infancy with migrating focal seizures. Nat. Commun. *6*, 8038.

Tamamaki, N., Yanagawa, Y., Tomioka, R., Miyazaki, J., Obata, K., and Kaneko, T. (2003). Green fluorescent protein expression and colocalization with calretinin, parvalbumin, and somatostatin in the GAD67-GFP knock-in mouse. J. Comp. Neurol. *467*, 60–79.

Tyzio, R., Represa, A., Jorquera, I., Ben-Ari, Y., Gozlan, H., and Aniksztejn, L. (1999). The establishment of GABAergic and glutamatergic synapses on CA1 pyramidal neurons is sequential and correlates with the development of the apical dendrite. J. Neurosci. *19*, 10372–10382.

Tyzio, R., Holmes, G.L., Ben-Ari, Y., and Khazipov, R. (2007). Timing of the developmental switch in GABA(A) mediated signaling from excitation to inhibition in CA3 rat hippocampus using gramicidin perforated patch and extracellular recordings. Epilepsia *48* (*Suppl 5*), 96–105.

Tyzio, R., Minlebaev, M., Rheims, S., Ivanov, A., Jorquera, I., Holmes, G.L., Zilberter, Y., Ben-Ari, Y., and Khazipov, R. (2008). Postnatal changes in somatic gamma-aminobutyric acid signalling in the rat hippocampus. Eur. J. Neurosci. *27*, 2515–2528.

Valeeva, G., Valiullina, F., and Khazipov, R. (2013). Excitatory actions of GABA in the intact neonatal rodent hippocampus in vitro. Front. Cell. Neurosci. *7*, 20.

Vanhatalo, S., Palva, J.M., Andersson, S., Rivera, C., Voipio, J., and Kaila, K. (2005). Slow endogenous activity transients and developmental expression of K+-Cl- cotransporter 2 in the immature human cortex. Eur. J. Neurosci. *22*, 2799–2804.

Verheugen, J.A., Fricker, D., and Miles, R. (1999). Noninvasive measurements of the membrane potential and GABAergic action in hippocampal interneurons. J. Neurosci. *19*, 2546–2555.

Vilen, H., Eerikäinen, S., Tornberg, J., Airaksinen, M.S., and Savilahti, H. (2001). Construction of gene-targeting vectors: a rapid Mu in vitro DNA transposition-based strategy generating null, potentially hypomorphic, and conditional alleles. Transgenic Res. *10*, 69–80.

Villette, V., Guigue, P., Picardo, M.A., Sousa, V.H., Leprince, E., Lachamp, P., Malvache, A., Tressard, T., Cossart, R., and Baude, A. (2016). Development of early-born γ-aminobutyric acid hub neurons in mouse hippocampus from embryogenesis to adulthood. J. Comp. Neurol. *524*, 2440–2461.

STAR★METHODS

KEY RESOURCES TABLE

REAGENT or RESOURCE	SOURCE	IDENTIFIER
Antibodies		
Anti-K+/Cl$^-$ Cotransporter (KCC2) Antibody	Merck Millipore	Cat #: 07-432, RRID:AB_310611
Alexa Fluor 568 goat anti-rabbit IgG (H+L)	Thermo Fisher	Cat #: A11036, RRID:AB_10563566
DAPI	Thermo Fisher	Cat #: D1306, RRID:AB_2629482
Streptavidin conjugated to Alexa Fluor 488	Thermo Fisher	Cat #: S11223, RRID:AB_2336881
Chemicals, Peptides, and Recombinant Proteins		
Alexa Fluor 488 NHS Ester (Succinimidyl Ester)	Thermo Fisher	Cat #: A20000
Biocytin	Sigma	Cat #: B4261
Bumetanide	Tocris	Cat #: 3108
CNQX disodium salt	Tocris	Cat #: 1045
D-AP5	Tocris	Cat #: 0106
DMSO	Sigma-Aldrich	Cat #: D8418
DPNI-gaged GABA	Tocris	Cat #: 2991
8-DMAQ GABA	Peter Dalco, Paris, Descartes University	N/A
Fluoromount-G	Thermo Fisher	Cat #: 00-4958-02
Gramicidin	Sigma-Aldrich	Cat #: G0550000
Picrotoxin	Tocris	Cat #: 1128
QX314 bromide	Tocris	Cat #: 1014
Tissue-Tek	Sakura Finetek	Cat #: 4583
TTX citrate	Tocris	Cat #: 1069
VU0463271	Tocris	Cat #: 4719
Experimental Models: Organisms/Strains		
Mouse: ICR (Hsd:ICR(CD-1))	Envigo	N/A
Mouse: GAD67-GFP	Tamamaki et al., 2003	N/A
Mouse: KCC2 $^{-/-}$	Vilen et al., 2001	N/A
Rat: Wistar (RccHan:WIST)	Envigo	N/A
Software and Algorithms		
Clampfit	Molecular Devices	https://www.moleculardevices.com/
FIJI	Schindelin et al., 2012	http://fiji.sc/
SPSS statistics	IBM	https://www.ibm.com/products/spss-statistics
MiniAnalysis	Synaptosoft	http://www.synaptosoft.com/MiniAnalysis/
Patchmaster	HEKA	https://www.heka.com/
WinEDR	Stratchlyde	http://spider.science.strath.ac.uk/sipbs/software_ses.htm

CONTACT FOR REAGENT AND RESOURCE SHARING

Further information and requests for resources and reagents should be directed to and will be provided by the Lead Contact, Kai Kaila (kai.kaila@helsinki.fi).

EXPERIMENTAL MODEL AND SUBJECT DETAILS

Wistar rats (P0-2, P5 and P17), ICR mice (P0-1) and KCC2$^{+/+}$, KCC2$^{-/-}$ (Vilen et al., 2001; Li et al., 2007; Puskarjov et al., 2014) and GAD67-GFP (Tamamaki et al., 2003) mice (E17.5-18.5) of either sex were used for the experiments. KCC2 full knock-out mice die at birth due to respiratory failure (Hübner et al., 2001), thus the experiments with KCC2$^{-/-}$ mice were limited to the above prenatal

period (see also Khalilov et al., 2011). For the collection of mouse embryos, timed pregnant mice dams were anesthetized with halothane and pups were delivered with C-section. Animals were housed in a conventional animal facility with a 12:12-hour light-dark cycle. The animals had access to food and water *ad libitum*. All experiments were approved by the Local Animal Ethics Committee of the University of Helsinki.

METHOD DETAILS

Hippocampal preparations

For the preparation of hippocampal slices, following decapitation, the brain was quickly removed and immersed into ice cold (< 4°C) cutting solution containing in mM: 87 NaCl, 2.5 KCl, 0.5 $CaCl_2$, 25 $NaHCO_3$, 1.25 NaH_2PO_4, 7 $MgCl_2$, 50 sucrose, and 25 D-glucose (310 ± 5 mOsm). Horizontal brain slices (400-450 μm-thick) containing the ventral hippocampus in transverse section were cut using a vibrating microtome (7000 SMZ-2; Campden Instruments). To obtain intact hippocampal preparations (Khalilov et al., 1997a) from mouse embryos, brains were dissected in ice-cold cutting solution. After removing the cerebellum, the hemispheres were separated. The deeper parts of the brain (brainstem, midbrain, and striatum) were carefully removed and the hippocampi were gently separated from the neocortex using two spatulas. Both the acute hippocampal slices and intact hippocampi were left to recover for 1 hr at 34°C in standard solution containing in mM: 124 NaCl, 3 KCl, 2 $CaCl_2$, 25 $NaHCO_3$, 1.1 NaH_2PO_4, 1.3 $MgSO_4$, and 10 D-glucose (300 ± 5 mOsm), after which they were stored in room temperature. All the extracellular solutions used in the study were equilibrated with carbogen (95% O_2, 5% CO_2).

Electrophysiological recordings

After recovery, hippocampal preparations were transferred to a submerged recording chamber maintained at 32 ± 1°C. The preparations were constantly perfused with standard physiological solution in which [K^+] was 3.5 mM (rat) and 4 mM (mouse). Perfusion rates of 3.5 ml/min or 5.0 ml/min were used for slices and hippocampi, respectively. The following drugs (all from Tocris) were supplemented to the extracellular solution when indicated: D-AP5 20 μM, CNQX 10 μM, TTX 0.5 μM, picrotoxin 100 μM, bumetanide 2.5 μM or 10 μM and VU0463271 10 μM. Bumetanide and VU0463271 were taken from 100 and 50 mM DMSO stocks, respectively. The DMSO vehicle (0.02%–0.1%) did not affect GDPs in either rats or mice (rats, fold change: 1.01 [IQR 0.87 – 1.15], [n = 6], p = 0.753; $KCC2^{+/+}$ mice, fold change: 1.001 [IQR 0.81 – 1.67], [n = 6], p = 0.6, Wilcoxon signed-rank test).

Local field-potential recordings were obtained either with a custom-made amplifier or an EXT-02B amplifier (npi electronic GmbH), using thin-filament glass-capillary pipettes (tip diameter 3-8 μm) filled with 150 mM NaCl placed in the pyramidal layer of area CA3. Data were stored using WinEDR (Strathclyde Electrophysiology) with a sampling rate of 2-5 kHz, 5 kHz low-pass filtering and 1000x amplification.

Single-cell recordings from visually-identified CA3 pyramidal neurons were obtained at a sampling rate of 20–50 kHz using an EPC 10 patch-clamp amplifier running Patchmaster software (HEKA). Borosilicate patch pipette resistance ranged from 3 to 6 MΩ. All voltages have been corrected for the respective liquid junction potentials (LJP). Series-resistance compensation (up to ~50%) was performed online.

For whole-cell voltage-clamp recordings of sIPSCs, all cells included in the analyses had a resting membrane potential more negative than −55 mV and a stable holding current. Recordings in which the access resistance (R_a) was higher than 30 MΩ or changed > 30% were not included in the analysis. The patch pipettes were filled with the following solution (in mM): 140 CsCl, 10 HEPES, 5 EGTA, 4 NaCl, 1 $CaCl_2$, 2 Mg-ATP, 5 QX314 bromide (pH adjusted to 7.2 with CsOH, 287 ± 5 mOsm, calculated LJP 3.9 mV). Neurons were held at a holding potential of −70 mV and ionotropic glutamate receptor blockers D-AP5 and CNQX were added to the extracellular solution.

Recordings of pyramidal neuron spiking were performed in loose cell-attached configuration (seal resistance 20-30 MΩ), using patch pipettes filled with extracellular solution. Baseline spiking rates were recorded with the DMSO vehicle in the extracellular solution.

To assess the efficacy of Cl^- extrusion in neonatal CA3 pyramidal neurons, we utilized our standard assay where a constant Cl^- load is imposed on the neuron via a pipette (5-6 MΩ tip resistance) patched onto the soma in whole-cell configuration (Khirug et al., 2005; Li et al., 2007; Puskarjov et al., 2015; Puskarjov et al., 2017; Spoljaric et al., 2017). In the presence of active Cl^- extrusion in the dendritic compartment, the deviation of the measured E_{GABA} from the $E_{GABA\text{-}GHK}$ predicted by the GHK voltage equation for Cl^- and HCO_3^- (the two anions permeating $GABA_A$Rs), becomes more negative with increasing distance from the somatic load (Khirug et al., 2005; Chamma et al., 2013). The pipette solution which had a Cl^- concentration of 19 mM consisted of (in mM): 18 KCl, 111 K-gluconate, 0.5 $CaCl_2$, 2 NaOH, 10 D-glucose, 10 HEPES, 2 Mg-ATP, 5 BAPTA and 0.1 Alexa Fluor 488; pH was adjusted to 7.3 with KOH, 283 ± 5 mOsm, calculated LJP 14 mV. Under these conditions, $E_{GABA\text{-}GHK}$ is set to −47.7 mV. The extracellular solution contained D-AP5, CNQX, and bumetanide (2.5 μM). $GABA_A$ receptor-mediated currents were elicited using local UV-photolysis (372 nm, 1-5 ms flash, 2 mW) of caged GABA (DPNI-GABA [Tocris] or 8-DMAQ-GABA [a kind gift of Peter Dalko, Paris Descartes University]) (0.5-1 mM). Caged GABA was dissolved with the above drugs and delivered to the slice at a flow rate of 1 μl/min via an UltraMicroPump II equipped with a syringe and a 100 μm inner tip-diameter quartz needle (WPI). E_{GABA} values were determined from current–voltage plots, obtained by sequentially stepping the membrane potential from the holding potential of −65 mV first to −95 mV for 700 ms and to a total six different levels with 10 mV increments and a 10 s step interval. Caged GABA was photolyzed

120 ms after the start of each voltage step to evoke $GABA_AR$-mediated currents at the soma and on the apical dendrite at a distance of 50 or 200 μm. Apical dendrites were traced using confocal microscopy of the Alexa Fluor 488 signal. In neurons where dendritic uncaging was performed at 200 μm from the soma (see Results), control E_{GABA} values were recorded in the presence of DMSO vehicle after which the perfusion solution was switched to that containing VU0463271 for 15 min before E_{GABA} values were determined in the same neuron. To ensure a constant Cl^- load from the pipette, recordings with change in R_a less than 20% were accepted for analysis.

In gramicidin-perforated patch recordings (Kyrozis and Reichling, 1995) of GABAergic mIPSCs the pipette solution consisted of the following (in mM): 55 K_2SO_4, 49 KCl, 0.5 $CaCl_2$, 5 EGTA, 10 HEPES and 0.1 Alexa Fluor 488 (pH adjusted to 7.2 with KOH, osmolarity adjusted with sucrose to 316 mOsm, calculated LJP 8 mV). Gramicidin (Sigma) (5 μg/ml) was added fresh to the pipette solution. The extracellular solution was supplemented with TTX, D-AP5 and CNQX. Recordings were started after the access stabilized. Access was monitored throughout the recording. To minimize clamping errors, pyramidal neurons were held at the potential where the holding current was zero, and kept at this potential throughout the recording. After a baseline of 5 min, VU0463271 was applied for 10 min via the bath perfusion. In the control recordings, DMSO (0.2 μl/ml) was applied instead of VU0463271.

Analysis of electrophysiological recordings

All events clearly distinguishable as GDPs were manually detected and their area (mV × ms) was quantified using numerical integration for each event in Clampfit (Molecular Devices). The event areas were assigned to 10 s bins according to the temporal sequence of the events to obtain the total area for each bin. For detailed analysis of the effect of VU0463271 on the frequency and analysis of GDPs, see Figure S3. IPSCs were analyzed with Mini Analysis (Synaptosoft) using a threshold of four-five × baseline RMS noise. Spiking frequencies recorded in loose cell-attached configuration were detected with WinEDR (Strathclyde). MUA was detected with Clampfit, after band-pass filtering > 400 and < 4000 Hz, using a threshold of 3.5 SD x baseline noise.

Immunohistochemistry

Brains from E18.5 $KCC2^{-/-}$, $KCC2^{+/+}$ and GAD67-GFP mice were fixed for two nights in PFA (4%, in PBS, pH 7.4) at +4°C, embedded in Tissue-Tek (Sakura Finetek, NL) and cut into 40 μm horizontal cryosections on a Leica CM1900 cryostat. The sections were washed (3 × 5 min in PBS), and blocking and was done in 3% BSA, 0.3% Triton-X, and 10% goat serum in PBS. The sections were incubated at +4°C overnight in blocking solution with the primary antibody against KCC2 (07-432, Millipore, 1:1000), and subsequently washed (3 × 5 min in PBS) and incubated 2 hr in room temperature with the secondary antibody (Alexa Fluor 568, Thermo Fisher, 1:500) in modified blocker solution (1% BSA, 0.3% Triton-X, 10% goat serum in PBS). The sections were then washed (3 × 5 min in PBS) and nuclei were visualized with DAPI (4', 6-Diamino-2-Phenylindole, Thermo Fisher, 1:2000 in PBS, 10 min incubation in room temperature). After the final washes the sections were mounted on glass slides with FluoromountG (Thermo Fisher). For analysis of KCC2 immunostaining, approximately 20 interneurons and pyramidal neurons per GAD67-GFP brain slice (n = 10 slices) were selected. The images were analyzed in FIJI (Schindelin et al., 2012). After outlining the neurons, the ROIs were overlaid on the KCC2 staining from the same slice. Neurons that showed KCC2 in the vicinity of the plasma membrane were marked as KCC2 positive. In some experiments, neurons from P0-1 ICR mouse acute brain slices (n = 7 slices) were filled with biocytin to better visualize somata for detection of KCC2 expression. For post hoc staining of individual neurons, biocytin (Sigma, 2.4 mg/ml) was added to the pipette solution containing (in mM) 29 KCl, 101 K-gluconate, 0.5 $CaCl_2$, 5 BAPTA, 10 HEPES, 10 glucose, 2 Mg-ATP, and 2 NaOH, with pH adjusted to 7.3 with KOH (280 ± 5 mOsm). Cells were filled for 2-5 min in the whole cell current-clamp configuration (I = 0 pA) to allow biocytin to diffuse into the neuron. Slices were post-fixed in PFA (4%, in PBS, pH 7.4) at +4°C overnight before staining. All the immunostainings were performed as in the cryosections from the embryos (see above). To visualize the biocytin, streptavidin-conjugated Alexa Fluor 488 (Thermo Fisher, 1:500) was added during the incubation with secondary antibodies. Images were taken using a Zeiss LSM 700 confocal microscope, equipped with LD LCI Plan-Apochromat 25x/0.8 Imm Corr and LD LCI Plan-Neofluar 63x/1.3 Imm Corr objectives.

QUANTIFICATION AND STATISTICAL ANALYSIS

All data are presented as median values with interquartile range (IQR). The n values provided in the figure panels or in the text indicate the number of cells or slices in single-cell and LFP recordings, respectively. Statistical analysis was done with SPSS Statistics (IBM). Wilcoxon signed-rank test and Mann-Whitney U test were used for statistical analysis between paired and independent samples, respectively. Friedman's two-way analysis of variance by ranks test was used to analyze the significance of multiple paired samples (Figure 2C). p values below 0.05 were considered as statistically significant, except in Figure 2C, where a Bonferroni adjusted p value of 0.025 was used to correct for false positives in multiple post hoc comparisons with Wilcoxon signed-rank test.

In single-cell recordings on VU0463271 drug actions, data were normalized to the last 5 min of pre-application baseline. In LFP experiments, the last 10 min of baseline were used for normalization in rats and, due to the much lower frequency of GDPs, to the last 20 min in mice. Quantification of the effect of bath-applied VU0463271 on all presented parameters is described as median from 10-15 min (whole-cell and loose cell-attached) or median from 5-10 min (gramicidin-perforated patch) after drug application in single-cell recordings median from 10-20 min in rat LFP recordings and median from 10-30 min in mouse LFP recordings. Quantification of DMSO effects on all parameters was done in the same time window as the drug effects.